THE STRUCTURAL DESIGN OF TALL AND SPECIAL BUILDINGS
Struct. Design Tall Spec. Build. **20**, 515–537 (2011)
Published online 18 December 2009 in Wiley Online Library (wileyonlinelibrary.com/journal/tal). DOI: 10.1002/tal.563

Use of rotational friction dampers to enhance seismic and progressive collapse resisting capacity of structures

J. Kim[1], H. Choi[1] and K.-W. Min[2*,†]

[1] *Department of Architectural Engineering, Sungkyunkwan University, Suwon, South Korea*
[2] *Department of Architectural Engineering, Dankook University, Yongin, South Korea*

SUMMARY

Passive energy dissipation devices are generally used to reduce structural responses caused by earthquake or wind loads. This study presents combined system of rotational friction dampers connected to high strength tendons to enhance both seismic and progressive collapse-resisting capacity of existing structures. Friction dampers were designed using the capacity spectrum method to satisfy given performance objectives against seismic load, and their seismic- and progressive collapse-resisting capacities were investigated. According to the nonlinear dynamic analysis results, the structures retrofitted with rotational friction dampers generally satisfied the given performance objectives against seismic load. Both the nonlinear static and dynamic analysis results showed that the progressive collapse potential of the model structures was significantly enhanced as a result of the seismic retrofit. Copyright © 2009 John Wiley & Sons, Ltd.

1. INTRODUCTION

There exist several alternative methods for the seismic upgrade of a building (ATC, 1996). The conventional methods of stiffening by adding concrete shear walls or rigid steel bracing tend to attract higher ground accelerations causing higher inertial forces on the supporting structure. Addition of new shear walls may interfere with the interior plan, and the energy dissipation capacity of a steel bracing system is very limited. Both conventional methods of upgrade require expensive and time-consuming work of strengthening the existing columns and foundations. In this sense, supplemental damping in conjunction with appropriate stiffness offers an economic solution for the seismic rehabilitation of building structures.

Friction dampers are considered as one of the most efficient energy-absorbing devices for building structures against earthquake load. As soon as the structure undergoes lateral deformations, the friction dampers are activated and start dissipating energy. Since the dampers may dissipate a major portion of the seismic energy, the forces acting on the structure can be considerably reduced. In contrast to shear walls or steel braces, the friction-dampers need not be vertically continuous. Since the damped bracing do not carry gravity load, they do not need to go down through the basement to the foundation. Friction dampers have been successfully applied to seismic retrofit of real structures (Pasquin *et al.*, 2002). Mualla and Belev (2002) proposed a friction damping device (FDD) and carried out tests for assessing the friction pad material, damper unit performance and scaled model frame response to lateral harmonic excitation. Moreschi and Singha (2003) presented a methodology to determine the optimal design parameters for the devices installed at different locations in a building for a desired performance objective. Bhaskararao and Jangid (2006) proposed numerical models of friction dampers for MDOF structures and validated the results with those obtained from an analytical model. Results show that using friction dampers to connect adjacent structures of different fundamental frequencies can effectively reduce earthquake-induced responses of either structure if the slip force of the dampers is appropriately selected. Lee *et al.* (2008) proposed a design methodology of combined system of bracing and friction dampers for seismic retrofit of structures.

*Correspondence to: Kyung-Won Min, Department of Architectural Engineering, Dankook University, Jukjeon-dong 126, Suji-gu, Yongin-si, Gyeonggi-do 448-701, South Korea
†E-mail: kwmin@dankook.ac.kr

Progressive collapse is a series of local and global failures due to local damage to structural elements caused by abnormal loads. The potential abnormal loads that can trigger progressive collapse are categorized as: aircraft impact, design/construction error, fire, gas explosions, accidental overload, hazardous materials, vehicular collision, bomb explosions, etc. (NIST, 2006). Kim and Kim (2009) showed that nonseismically designed low-rise structures could be vulnerable to progressive collapse especially when a first-storey corner column was removed. Hayes *et al.* (2005) investigated the relationship between the seismic design and the blast or progressive collapse-resisting capacity and mentioned that the special moment frame detailing provisions required in areas of high seismicity would provide better resistance to external explosion or impact effects than the less-rigorous detailing required for Ordinary Moment-resisting Frames (OMF). To resist progressive collapse of structures, Crawford (2002) proposed the use of connection details developed for earthquake such as Side Plate™, the use of cables imbedded in reinforced concrete beams to activate the catenary action, and the use of mega-truss in high-rise buildings. Kim and An (2009) investigated the progressive collapse potential of steel moment frames considering catenary action of beams assuming that the joints are strong enough to resist the catenary force.

This study presents the performance of friction dampers connected to high strength tendons to enhance both seismic and progressive collapse resisting capacity of existing structures. To this end 3-, 6- and 15-storey reinforced concrete moment frames were designed considering only gravity loads. Rotational friction dampers were designed using the capacity spectrum method to satisfy given performance objectives against seismic load, and their seismic and progressive collapse resisting capacity were investigated using nonlinear static and dynamic analyses.

2. INSTALLATION OF ROTATIONAL FRICTION DAMPERS WITH CABLES

Mualla and Belev (2002) proposed rotational FDDs composed of a central steel plate, two side plates and two circular friction pad discs placed in between the steel plates as shown in Figure 1. The central plate is attached to the girder midspan in a framed structure by a hinge. The ends of the two side plates are connected to the members of inverted V-brace as shown in Figure 2. The bracing makes use of pretensioned bars in order to avoid compression stresses and subsequent buckling. The bracing bars are pin-connected at both ends to the damper and to the column bases. The combination of two side plates and one central plate increases the frictional surface area and provides symmetry needed for obtaining plane action of the device. A pretightened bolt connects the three plates of the damper to each other. This adjustable bolt is used to control the compression force applied on the interfaces

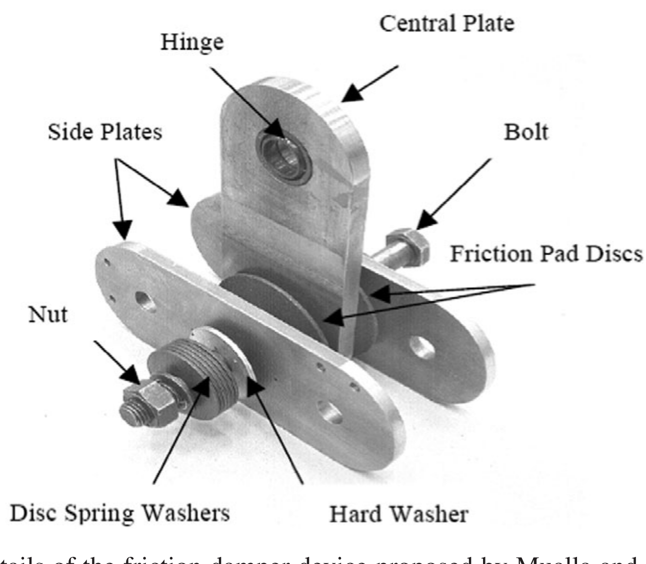

Figure 1. Details of the friction damper device proposed by Mualla and Belev (2002).

DOI: 10.1002/tal

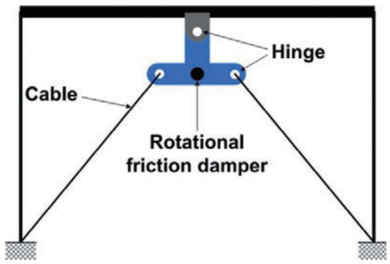

Figure 2. Installation of the friction damper and cables.

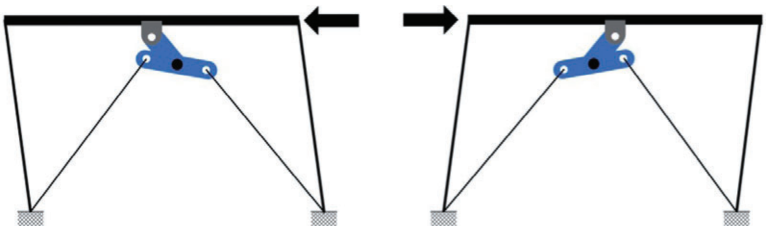

Figure 3. Mechanism of the rotational friction damper.

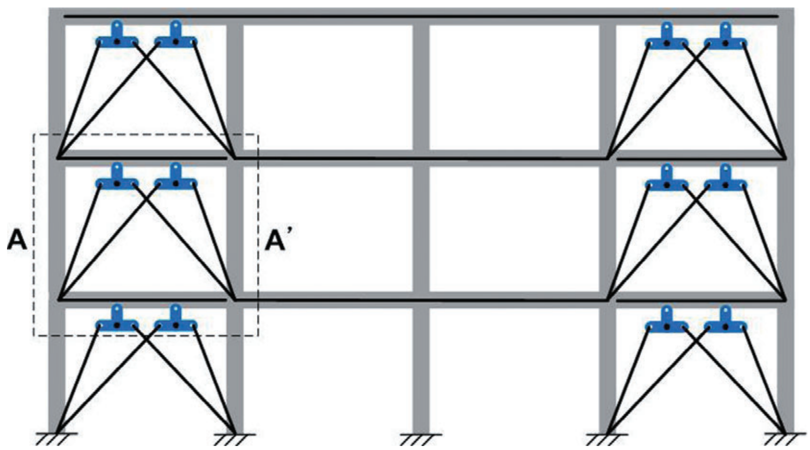

Figure 4. Structure with the friction devices installed with cables.

of the friction pad discs and steel plates. When a lateral force excites a frame structure, the girder tends to displace horizontally. The bracing system and the forces of friction developed at the interface of the steel plates and friction pads will resist the horizontal motion. Figure 3 depicts the functioning of the FDD under lateral excitation. Only tensile forces are induced in the cables. As is shown, the device is very simple in its components and can be arranged within different bracing configurations to obtain a complete damping system. Figure 4 depicts the installation scheme of FDDs with cables so that vertical deflections caused by sudden loss of a column as well as the lateral drifts by wind or seismic loads are also reduced. In the three-bay model structure two FDDs are placed in each of the end spans, and as the cables are continuous along the floor beams, all FDDs will be activated no matter which column is lost.

3. DESIGN OF FRICTION DAMPERS

3.1. Estimation of the required effective damping ratio

The damping ratio required to satisfy a given performance limit state can be conveniently obtained using the capacity spectrum method presented in the ATC-40 report (ATC, 1996). The first step for application of capacity spectrum method is to transform the structure to an equivalent single-degree-of-freedom (SDOF) structure. It also requires that both the demand spectra and structural capacity curve be plotted in the spectral acceleration S_a versus spectral displacement S_d domain, which is known as the acceleration–displacement response spectra (ADRS), using the following relationship:

$$S_a = \frac{V}{M_s^*}, \quad S_d = \frac{\Delta_{sR}}{\Gamma_s \phi_{sR}} \left(\phi_{si} = \sqrt{\sum_{j=1}^{N} (\phi_{ij})^2}, M_s^* = \frac{\left(\sum_{i=1}^{N} m_i \phi_{si}\right)^2}{\sum_{i=1}^{N} m_i \phi_{si}^2}, \Gamma_s = \frac{\sum_{i=1}^{N} m_i \phi_{si}}{\sum_{i=1}^{N} m_i \phi_{si}^2} \right) \tag{1}$$

where S_a and S_d are the acceleration and displacement responses, respectively; M_s^* and Γ_s are the effective mass and mass participation factor, respectively; ϕ_{sR} and ϕ_{si} represent the coefficients of the mode shape vector, combined by square root of sum of squares (SRSS) technique, corresponding to the roof and the *i*th storey, respectively; ϕ_{ij} is the *i*th coefficient of the *j*th mode shape vector; and m_i is the mass of the *i*th storey.

To convert a response spectrum with the standard acceleration versus natural period format to ADRS, it is necessary to determine the value of S_d corresponding to each point on the original curve. The relationship between the base shear and the top storey displacement is obtained by gradually increasing the lateral loads appropriately distributed over the stories. In this study, the effects of the higher modes are considered during pushover analysis by combining all modes using SRSS method. The lateral storey force is obtained as follows (Freeman *et al.*, 1998):

$$F_i = \sqrt{\sum_{j=1}^{N} \left(\frac{\sum_{i=1}^{N} m_i \phi_{ij}}{\sum_{i=1}^{N} m_i \phi_{ij}^2} \phi_{ij} S_{aj} m_i \right)^2} \tag{2}$$

where ϕ_{ij} is the *i*th component of the *j*th mode shape vector and S_{aj} is the spectral acceleration corresponding to the *j*th mode. If the inherent viscous damping of the structure is assumed to be ς_i, then the effective damping ratio of the system can be obtained as:

$$\varsigma_{eff} = \varsigma_i + \kappa \varsigma_{eq} \tag{3}$$

where ς_{eq} is the equivalent damping ratio contributed from hysteretic behaviour, and κ is the efficiency factor, which is taken to be 1.0 when perfect bilinear system is assumed. The effective damping is used to plot the demand curve. The equivalent viscous damping ratio of the structure subjected to hysteretic response shown in Figure 5 is determined from the energy dissipated by the hysteretic

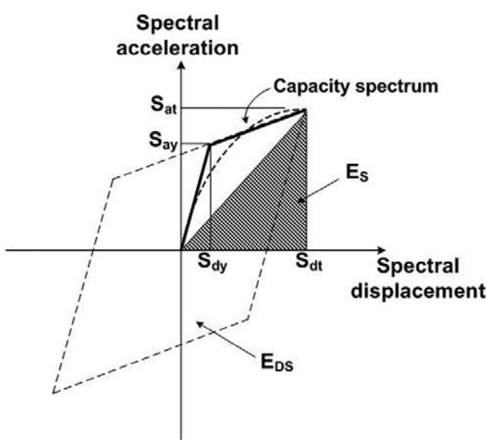

Figure 5. Estimation of equivalent damping ratio.

behaviour, E_D, which is the area enclosed by the hysteresis loop at maximum displacement, and the stored potential energy corresponding to the area of the shaded triangle, E_S (FEMA, 1997):

$$\zeta_{eq} = \frac{1}{4\pi}\frac{E_D}{E_S} = \frac{2(S_{ay}S_{dt} - S_{dy}S_{at})}{\pi S_{dt}S_{at}} \tag{4}$$

where the variables S_{ay} and S_{dy} are the acceleration and displacement of the equivalent SDOF system at yield, respectively, and S_{at} and S_{dt} are the acceleration and displacement at target point, respectively. A bilinear representation of the capacity spectrum is needed to estimate the effective damping and appropriate reduction of spectral demand.

When friction dampers with tendons are installed in a structure the stiffness as well as the damping ratio increases. This results in the change in the effective period (T_{eff}) and the capacity curve as depicted in Figure 6, where S_{dt} represents the target displacement of the equivalent SDOF system, and S_{at1} and S_{at2} are the maximum acceleration responses at the target displacementS_{at} before and after the damping system is installed. The effective damping ratio of a structure with added damping devices can be expressed as follows:

$$\varsigma'_{eff} = \varsigma_i + \kappa\varsigma'_{eq} + \varsigma_d \tag{5}$$

where ζ'_{eq} is the equivalent damping of the structure with damping device, and ς_d is the equivalent damping ratio contributed from the FDD. Based on Figure 5, ζ'_{eq} can be obtained as follows:

$$\varsigma'_{eq} = \frac{2(S_{ay}S_{dt} - S_{dy}S_{at1})}{\pi S_{at2}S_{dt}} \tag{6}$$

The energy dissipated by the FDD per loading cycle is equivalent to the area enclosed in the rectangular bending moment–rotation curve shown in Figure 7. The dissipated energy E_{DF} can be simplified

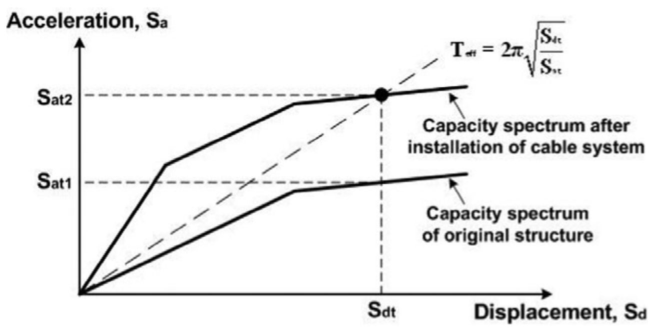

Figure 6. Changed capacity spectrum due to installation of FDD.

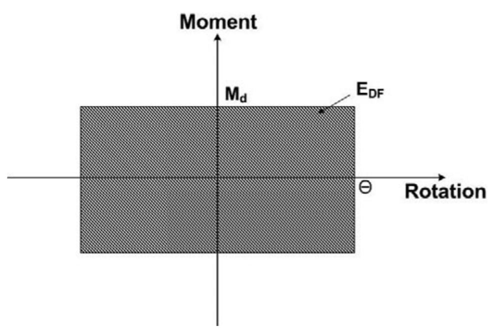

Figure 7. Energy dissipated by FDD.

DOI: 10.1002/tal

to Equation (7), and the equivalent damping ratio ς_d required to satisfy a given performance point can be obtained as Equation (8):

$$E_{DF} = \int M\theta d\theta = 4M_d\theta \tag{7}$$

$$\varsigma_d = \frac{1}{4\pi}\frac{E_{DF}}{E_S} = \frac{2M_d\theta}{\pi S_{at2}S_{dt}} \tag{8}$$

where E_S represents the maximum strain energy of the structure with damping system, M_d is the rotational frictional strength of the damping device, and θ is the rotation of the FDD.

3.2. Determination of frictional moment of FDD

Based on the assumption that the deformation of the dampers is equal to the interstorey drift of the structure, Equation (8) can be transformed into Equation (9):

$$\varsigma_d = \frac{2F_dS_{dt}}{\pi S_{at2}S_{dt}} \tag{9}$$

Using the above equation the rotational frictional moment can be determined as follows:

$$M_d = F_dh_a = \left(\frac{1}{2}\varsigma_d\pi S_{at2}\right)h_a \tag{10}$$

where h_a is the length of the vertical steel plate. To obtain the acceleration response increased by the addition of damping devices, S_{at2}, the stiffness added by the devices needs to be computed. As the strength of the tendons is generally very high, the yield strength of the combined damper + cable system depends only on the yield strength of the FDD as shown in Figure 8. It would simplify the design process to design the FDD so that their yield displacements are the same as the yield displacement of the structure. With the yield strength of the FDD defined, the yield strengths of the structure with the damping devices, F_{y1} and F_{y2}, can be obtained as follows using Figure 9:

$$F_{y1} = F_{cy} + K_su_{cy} = K_cu_{cy} + K_su_{cy} \tag{11}$$

$$F_{y2} = F_{cy} + F_{sy} \tag{12}$$

where u_{cy} and u_{sy} are the yield displacements of FDD and the structure, respectively, and F_{cy} and F_{sy} are the yield strength of the FDD and the structure, respectively. When dampers and tendons are installed as shown in Figure 4, the lateral stiffness contributed from the tendons can be obtaind as follows:

$$\begin{aligned} K_c = N(K_i + K_j) &= N\left\{\frac{E_cA_i}{L_i}\cos^2\theta_i + \frac{E_cA_j}{L_j}\cos^2\theta_j\right\} \\ &= N\left\{\frac{E_cA(L_i\cos^2\theta_j + L_j\cos^2\theta_i)}{L_iL_j}\right\} \end{aligned} \tag{13}$$

where N is the number of the dampers installed in a storey; E_c is the elastic constant of the tendon; A is the cross-sectional area of the tendon; θ_i and θ_j are the slopes of the tendons located in the left- and right-hand-side of the damper, respectively; and L_i and L_j are the length of the tendons located in the left- and right-hand-side of the damper, respectively. The capacity curve of the structure with FDD can be plotted as Figure 9 using the following relation:

DOI: 10.1002/tal

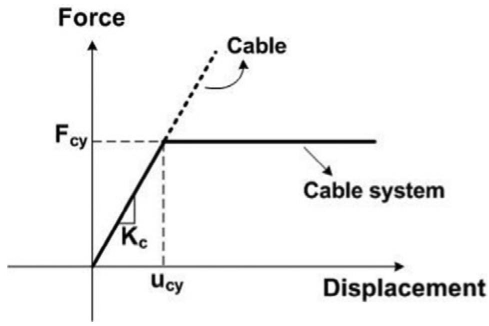

Figure 8. Force–displacement relationship of the cable system.

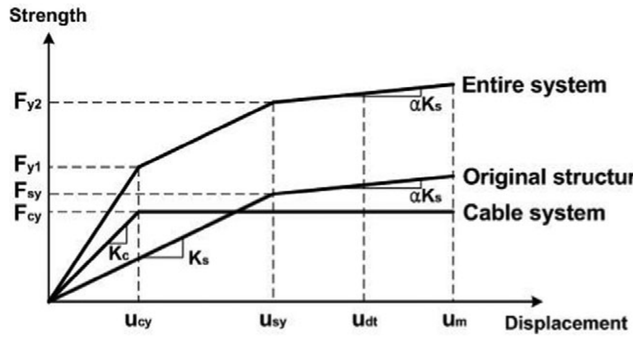

Figure 9. Force–displacement relationship of a structure with FDD.

$$S_{acy} = w_n^2 S_{dcy} = \frac{K_c^*}{M_s^*} S_{dcy} \tag{14}$$

where $K_c^* = \sum_{i=1}^{N} K_{ci}$ and n is the number of storey.

Finally, the effective damping ratio of the structure with FDD, ς'_{eff}, can be obtained from the capacity curve and the demand curve corresponding to the target displacement, and the additional damping ratio required to meet the performance objective, ς_d, can be obtained from Equation (5) as follows:

$$\varsigma_d = \varsigma'_{eff} - \varsigma_i - \kappa\varsigma'_{eq} \tag{15}$$

The required rotational friction moment of the damper can be computed by substituting ς_d into Equation (10). The above process is carried out after transforming the structure into the equivalent SDOF system, and therefore the required damping ratio obtained in Equation (15) needs to be distributed to each storey of the multistorey prototype structure. In this study, the required damping is distributed to each storey proportional to the interstorey drift obtained by pushover analysis.

4. DESIGN AND MODELLING OF ANALYSIS MODEL STRUCTURES

4.1. Design of analysis structures

To validate the design process of the dampers, 3-, 6- and 15-storey reinforced concrete model structures, shown in Figure 10, were designed (i) as ordinary moment-resisting frames (OMRF) without considering seismic load and (ii) as special moment-resisting frames (SMRF) considering seismic load. One of the horizontal external frames was taken out of the three- by four-bay moment resisting frames shown in Figure 11. The model structures were designed to have 8-m span length and the

DOI: 10.1002/tal

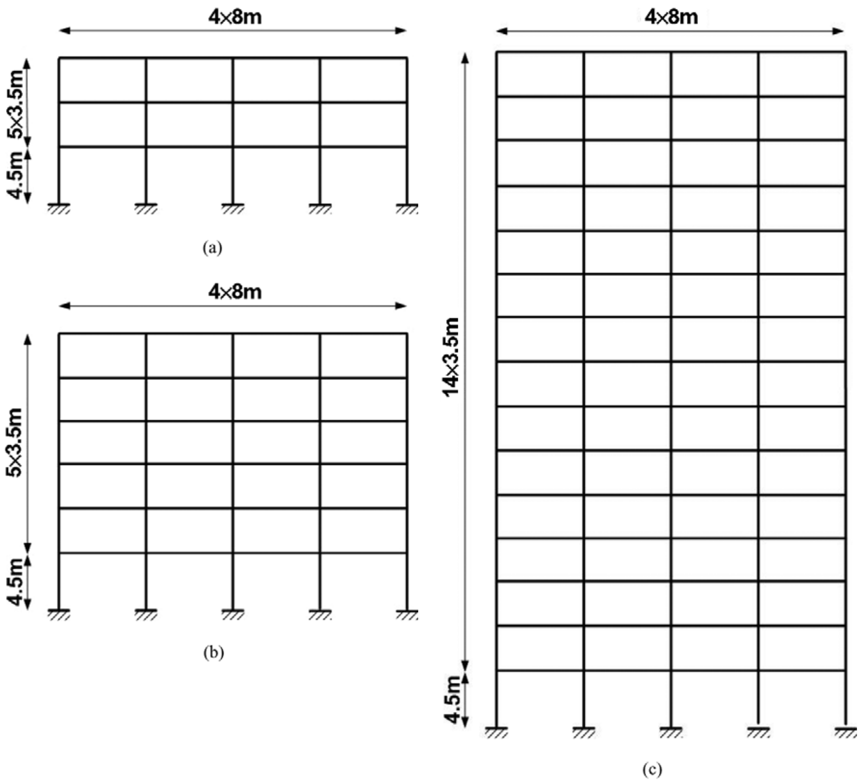

Figure 10. Elevation of analysis model structures: (a) three-storey; (b) six-storey; and (c) 15-storey.

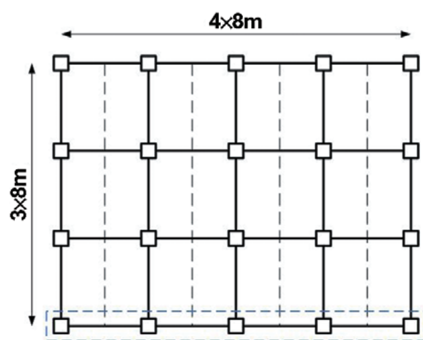

Figure 11. Structural plan of analysis model structure.

design dead and live loads were 4.5 kN/m^2 and 2.5 kN/m^2, respectively. Structural members were designed using normal strength concrete having f_c' = 2.4 kN/cm^2 in accordance with the ACI 318 (2002), and seismic load was determined based on the International Building Code (ICC, 2006). In the model structures the member sizes were varied in every three stories. The coefficients for design seismic load are presented in Table 1 and the member sizes of the designed model structures are shown in Table 2.

4.2. Modelling for analysis

The model structures were analysed using the program code OpenSees (Mazzoni *et al.*, 2007), which can simulate static and dynamic structural behaviours considering both material and geometric non-

DOI: 10.1002/tal

Table 1. Seismic design coefficients for model structures.

Maximum considered earthquake	$S_s = 1.61$ g, $S_1 = 0.79$ g
Site class	Class D, Stiff Soil: $F_a = 1.0$, $F_v = 1.5$
Design earthquake	$S_{DS} = 1.07\ g$, $S_{D1} = 0.79\ g$
Seismic use group	Group I: $I_E = 1.0$ (three-storey, six-storey)
	Group II: $I_E = 1.25$ (15-storey)
Seismic design category	D

Table 2. Member size and reinforcement used in the analysis models.

(a) Member size and reinforcement of beams.

Model	Type		Member Size (mm)	Reinforcing steel: End of beam: Top	End of beam: Bottom	Mid-span of beam: Top	Mid-span of beam: Bottom
3-storey	1–3 storey	S	450 × 600	4-D22	3-D19	2-D19	3-D19
		NS	450 × 550	4-D19	2-D19	2-D16	5-D16
6-storey	1–3 storey	S	500 × 650	6-D22	3-D25	2-D25	2-D25
		NS	450 × 550	4-D19	2-D19	2-D19	3-D19
	4–6 storey	S	450 × 600	5-D22	2-D25	2-D22	3-D25
		NS	450 × 550	4-D19	2-D19	2-D19	4-D19
15-storey	1–3 storey	S	550 × 650	6-D25	3-D29	3-D22	3-D22
		NS	550 × 650	4-D19	2-D19	2-D19	3-D19
	4–6 storey	S	520 × 630	6-D25	3-D29	2-D25	3-D22
		NS	520 × 630	4-D19	2-D19	2-D19	4-D19
	7–9 storey	S	500 × 600	6-D25	3-D29	2-D25	2-D25
		NS	500 × 600	4-D19	2-D19	2-D19	4-D19
	10–12 storey	S	500 × 570	5-D25	2-D29	2-D25	2-D25
		NS	500 × 570	4-D19	2-D19	2-D19	4-D19
	13–15 storey	S	430 × 540	10-D25	5-D25	2-D22	2-D25
		NS	430 × 540	4-D19	2-D19	2-D19	4-D19

(b) Member size and reinforcement of columns.

Model	Type		Exterior columns: Member Size (mm)	Exterior columns: Reinforcing steel	Interior columns: Member Size (mm)	Interior columns: Reinforcing steel
3-storey	1–3-storey	S	470 × 470	4-D29	550 × 550	12-D25
		NS	350 × 350	6-D19	400 × 400	10-D19
6-storey	1–3-storey	S	500 × 500	6-D29	600 × 600	12-D29
		NS	370 × 370	6-D19	450 × 450	8-D19
	1–3-storey	S	450 × 450	10-D25	570 × 570	12-D29
		NS	370 × 370	6-D19	450 × 450	8-D19
15-storey	1–3-storey	S	600 × 600	12-D25	700 × 700	10-D29
		NS	550 × 550	6-D25	700 × 700	10-D25
	4–6-storey	S	570 × 570	6-D32	670 × 670	14-D25
		NS	500 × 500	4-D29	650 × 650	12-D22
	7–9-storey	S	530 × 530	8-D32	630 × 630	12-D29
		NS	450 × 450	4-D25	620 × 620	6-D29
	10–12-storey	S	500 × 500	6-D32	620 × 620	12-D25
		NS	420 × 420	4-D25	570 × 570	6-D29
	13–15-storey	S	470 × 470	6-D29	570 × 570	12-D22
		NS	400 × 400	4-D25	520 × 520	6-D29

S, seismic design; NS, non-seismic design.

linearities. Beams and columns were modelled by 'nonlinearbeamcolumn element', and the tendons and FDD were modeled by 'corotTruss element' and 'zerolength element', respectively, using the 'ElasticPP material'. The hysteretic behaviour of structural steel and reinforcing bars was modelled by the 'Hysteretic material' as shown in Figure 12(a). The cover concrete and the core concrete were modelled by the 'Concrete01' and the 'Concrete02' materials, respectively, as shown in Figure 12(b). The behaviours of cover and core concrete were modelled based on the work of Mander *et al.* (1988). For dynamic analysis, 5% damping ratio was assumed and was implemented into the analysis using the Rayleigh method. Table 3 shows the dynamic properties of the model structures before installation of dampers.

4.3. Seismic response of the model structures retrofitted by friction dampers

In this section, the amount of FDD required to meet a given target displacement for a specific earthquake were estimated through the capacity-demand diagram procedure described above, and the seismic responses of the model structures retrofitted by the friction dampers were evaluated by nonlinear dynamic analyses. To construct demand curve an artificial earthquake with the peak ground acceleration equal to 0.5 *g* was generated based on the design spectrum with S_{DS} = 1.07 and S_{D1} = 0.79. Figure 13 plots the time history of the generated earthquake ground acceleration, and Figure 14

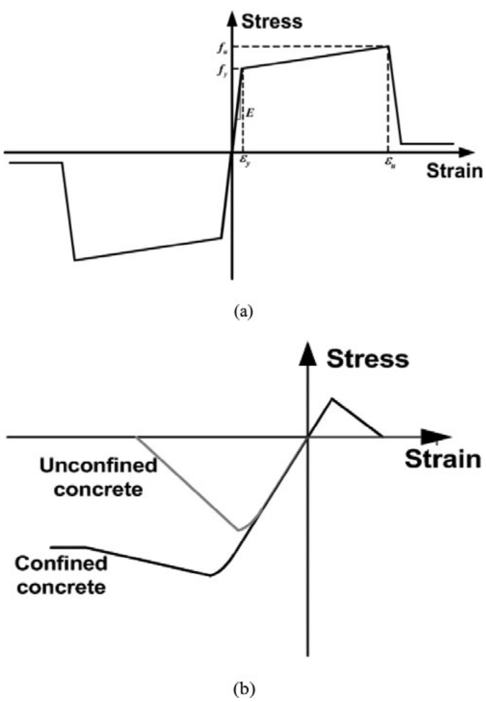

Figure 12. Stress–strain relationship of structural materials: (a) reinforcing steel; and (b) concrete.

Table 3. Modal properties for non-seismic designed structures.

Model	Vibration mode	1st	2nd	3rd
3-storey	Period (s)	0.68	0.20	0.11
	Effective mass (%)	95.5	4.06	0.4
6-storey	Period (s)	1.01	0.32	0.18
	Effective mass (%)	89.6	7.7	1.8
15-storey	Period (s)	1.60	0.58	0.34
	Effective mass (%)	77.8	12.3	4.3

DOI: 10.1002/tal

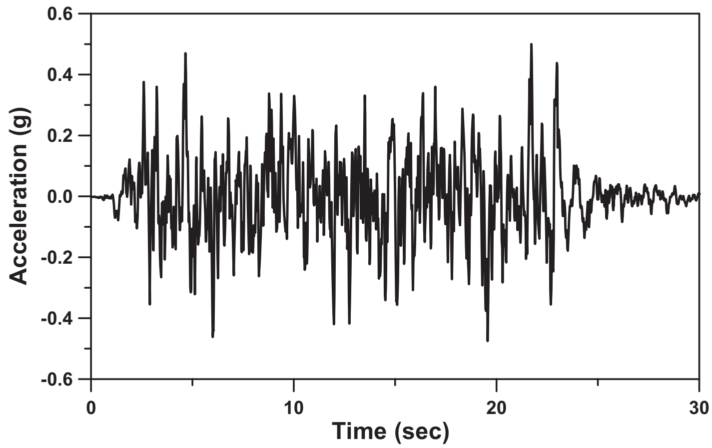

Figure 13. Time-history of artificial earthquake record.

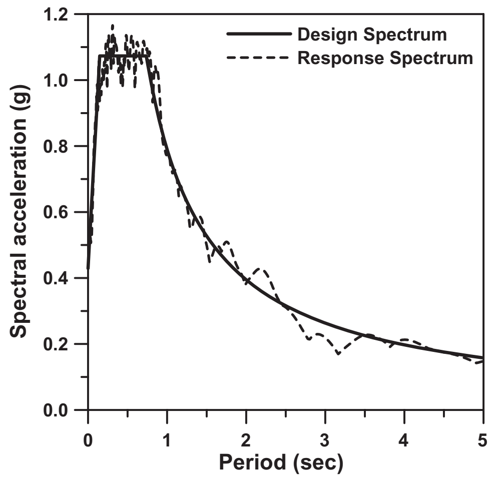

Figure 14. Response spectrum for artificial ground motion.

Table 4. Decision of target drift and top storey displacement.

Model	Target drift (%)	Top storey displacement (cm)
3-storey	1.5	10.01
6-storey	1.0	12.87
15-storey	0.5	18.92

shows the design spectrum and the response spectrum of the artificial record. The target performance points were determined based on the interstorey drift limit states. Different target point was assigned to each model structure to confirm the validity of the damper design process. Table 4 shows the given target interstorey drifts and the top storey displacements of the model structures at which the target drifts were reached.

Figures 15–17 show the procedure to estimate the required damping for each model structure to meet the target displacement. The estimated required damping ratios for the model structures are presented in Table 5. Figure 18 shows the top-storey displacement time-histories of the OMRF model

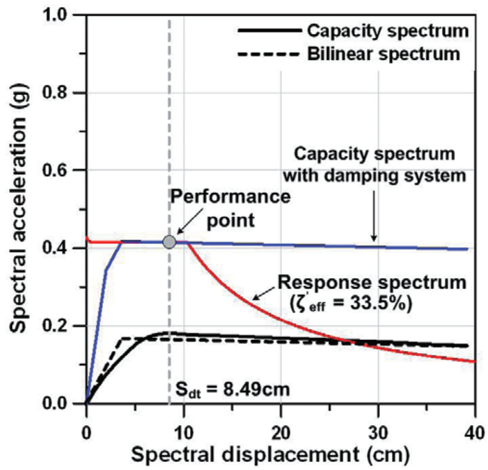

Figure 15. Estimation of required damping ratio for three-storey structure.

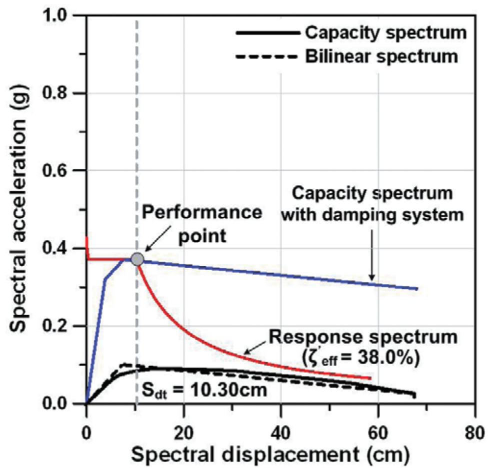

Figure 16. Estimation of required damping ratio for six-storey structure.

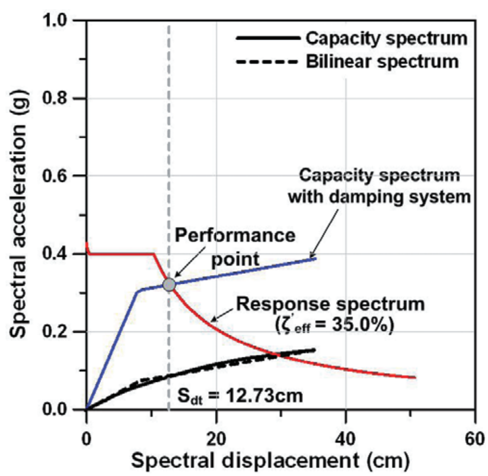

Figure 17. Estimation of required damping ratio for 15-storey structure.

DOI: 10.1002/tal

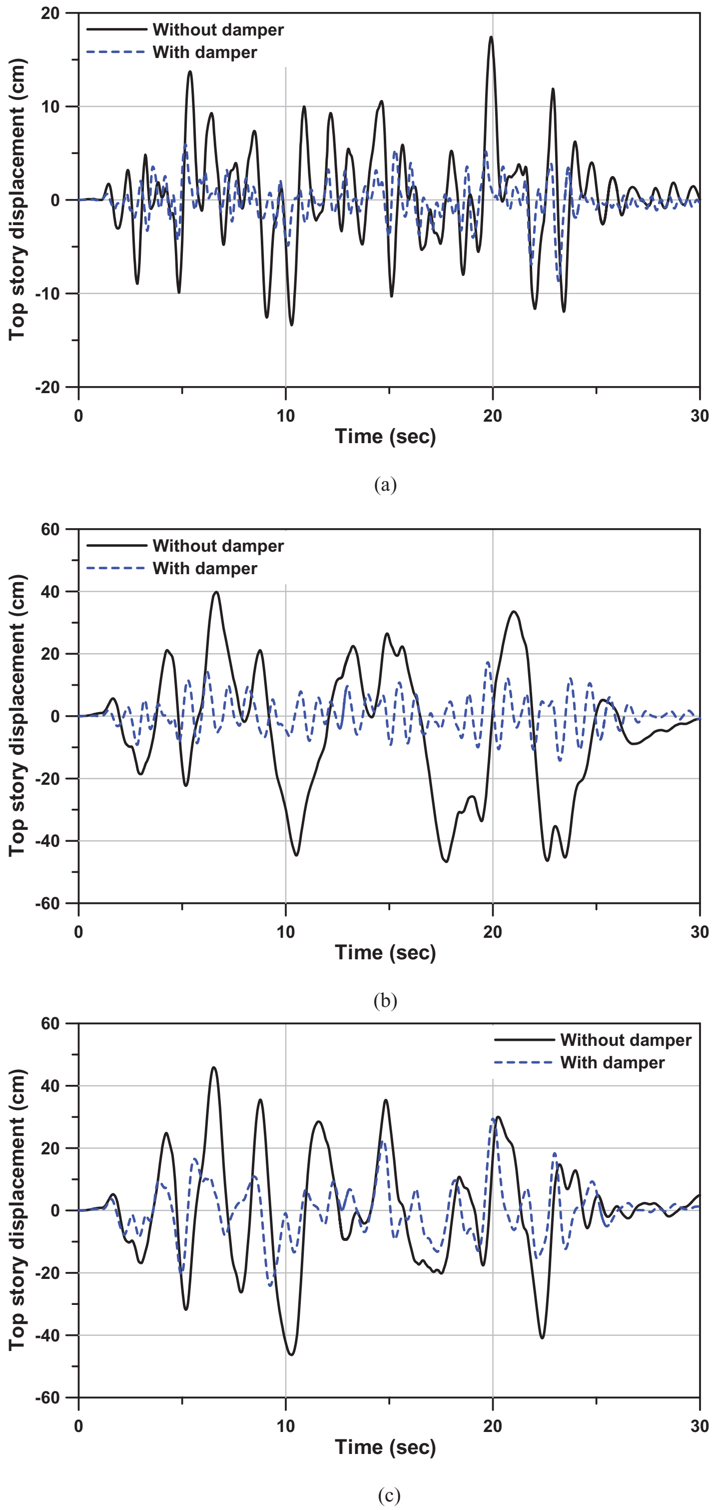

Figure 18. Time histories with and without FDD: (a) three-storey; (b) six-storey; and (c) 15-storey.

DOI: 10.1002/tal

Table 5. Estimation of required damping ratio and rotational frictional strength.

	Responses of equivalent SDOF system (ADRS format)								
	Displacement (cm)			Acceleration (g)					
Model	S_{cy}	S_{sy}	S_{dt}	$S_{at,1}$	$S_{at,2}$	S_{at}	ζ'_{eff} (%)	ζ_d (%)	M_d (kNcm)
3-storey	2.00	3.61	8.49	0.343	0.417	0.414	33.5	13.6	2599.7
6-storey	3.78	7.49	10.30	0.320	0.370	0.368	38.0	27.9	4730.3
15-storey	7.75	8.14	12.73	0.300	0.304	0.320	35.0	26.0	3846.9

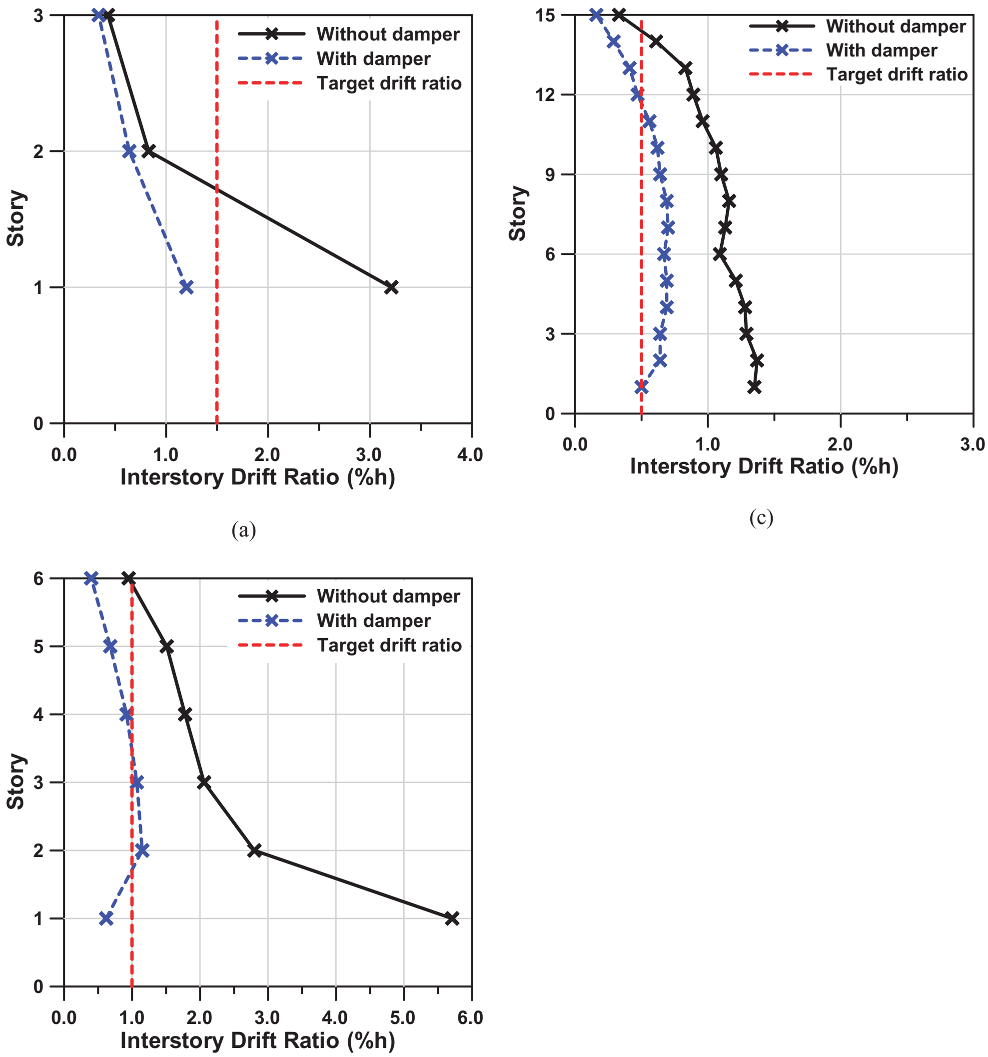

Figure 19. Variation of maximum interstorey drift ratio: (a) three-storey; (b) six-storey; and (c) 15-storey.

structures with and without the dampers. It can be observed that displacement responses decreased significantly with the addition of the dampers. The interstorey drifts of the model structures depicted in Figure 19 show that interstorey drifts decreased with the installation of the dampers and the target drifts are generally satisfied with the installation of the dampers. As the dampers are activated by the

DOI: 10.1002/tal

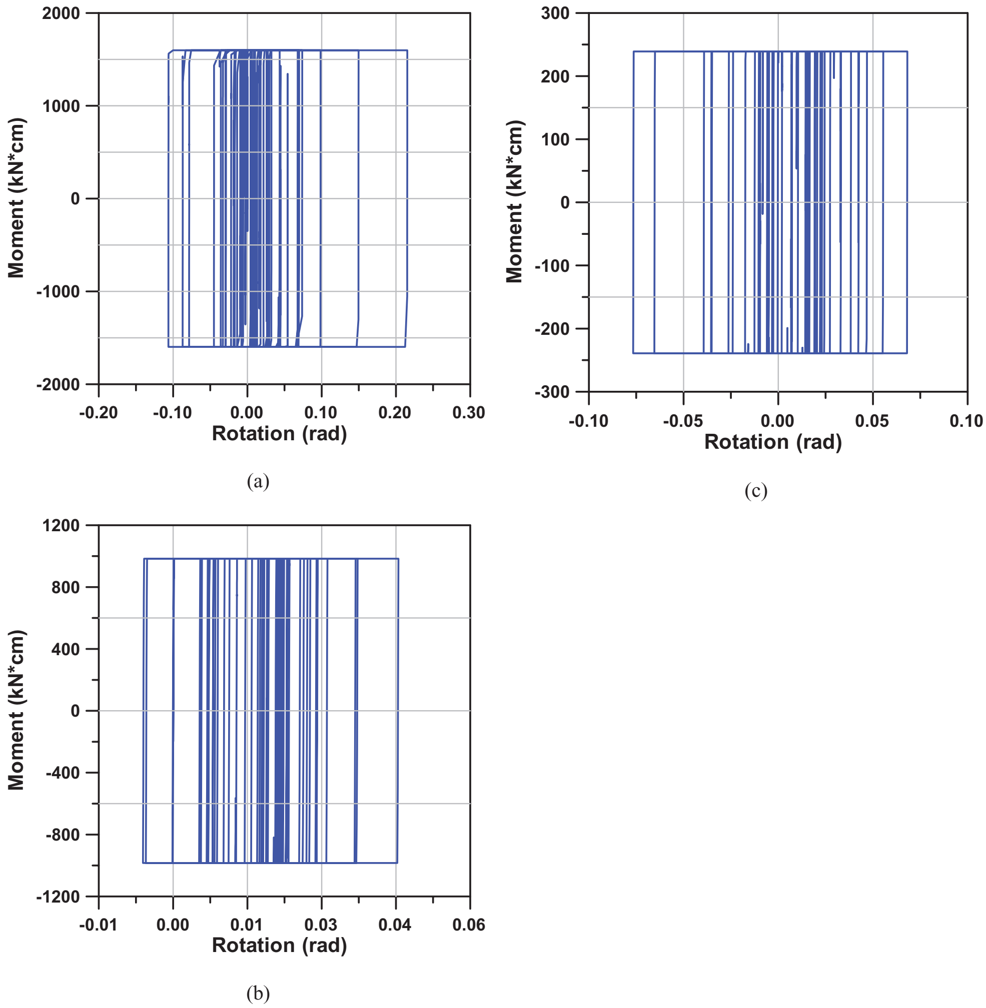

Figure 20. Behaviour of FDD under artificial earthquake: (a) three-storey; (b) six-storey; and (c) 15-storey.

occurrence of interstorey drift, they will be most effective when structures deform at shear beam mode. This may explain the excedence of the target drift in most stories of the 15-storey structure, which deforms in bending or cantilever mode in combination with the shear mode. Figure 20 shows the hysteresis curves of the FDD installed in the model structures. As expected, the dampers show stable hysteretic behaviour and dissipate large amount of seismic energy.

5. COLLAPSE PERFORMANCE OF RETROFITTED STRUCTURES

5.1. Analysis method for progressive collapse

Figure 21 shows the gravity load applied on the model structures for progressive collapse analysis. For static analysis, the USGSA guidelines (2003) recommends to use dynamic amplification factor of 2.0 in load combination in the bays from which a column is removed as shown in Figure 21(a). For dynamic collapse analysis no amplification factor was applied. To carry out dynamic analysis, the axial force acting on a column was computed first before the column was removed. Then the column was replaced by point loads equivalent of its member forces as shown in Figure 21(b). To simulate the effect of a column abruptly removed, the member forces were suddenly removed after a few seconds were elapsed as shown in Figure 21(c), where W is the vertical load.

DOI: 10.1002/tal

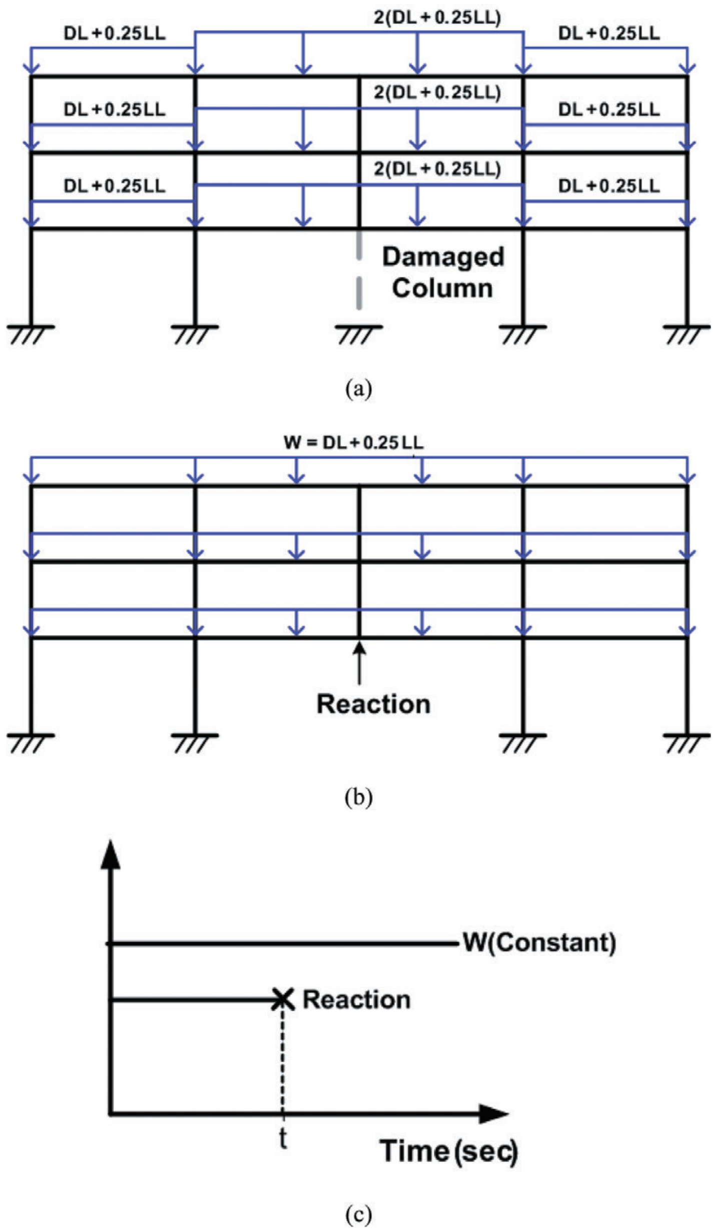

Figure 21. Applied load for progressive collapse analysis: (a) Gravity load applied for nonlinear static analysis; (b) Gravity load applied for nonlinear dynamic analysis; and (c) Application of vertical load for dynamic analysis.

5.2. *Equivalent truss element*

The tendons connected to the dampers in both the exterior bays are continued in the two interior bays as shown in Figure 5. When an interior column is suddenly removed, the dampers are activated by the tendons located parallel to the floor beams. The tendons were modelled as equivalent truss elements with the effective horizontal stiffness and member properties obtained as follows:

$$\frac{1}{k_{eff}} = \frac{1}{k_i \cos^2\theta_i} + \frac{1}{k_h}; \quad \frac{1}{\frac{E_c A_{eff}}{L_{eff}}} = \frac{1}{\frac{E_c A_i}{L_i}\cos^2\theta_i} + \frac{1}{\frac{E_c A_h}{L_h}} \tag{16}$$

DOI: 10.1002/tal

where A_i, L_i and θ_c are the cross-sectional area, length and slope of the sloping tendons connected to the dampers, respectively; A_h and L_h are the cross-sectional area and the length of the horizontal tendons, respectively; E_c is the elastic modulus of the tendon; and A_{eff} and L_{eff} are the cross-sectional area and the length of the equivalent truss elements, respectively. By equating L_{eff} with distance between the damper and the joint from which a column is removed, the effective cross-sectional area of the cable, A_{eff}, can be obtained.

5.3. Progressive collapse analysis results

The model structures with and without FDD were analysed with one of the first storey columns removed. In the SMRFs designed with seismic load, the sum of the nominal flexural strengths of the columns framing into a joint was selected to be at least 1.2 times larger than those of the beams framing into the joint to ensure strong column-weak beam mechanism. Figures 22–24 present non-

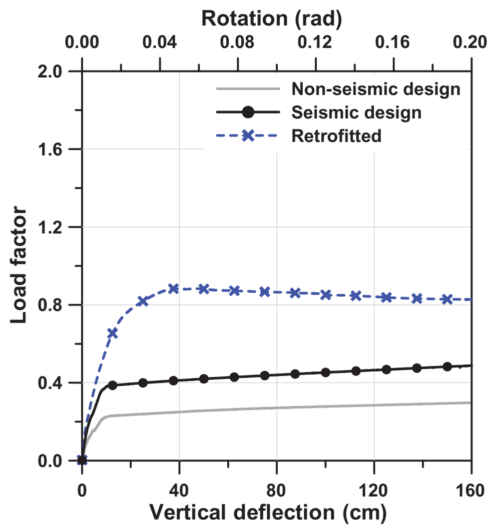

(a)

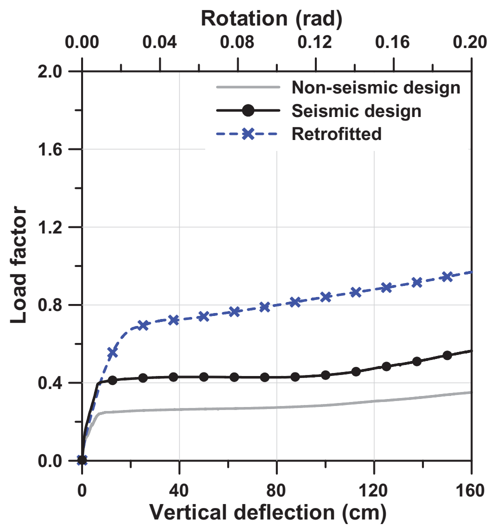

(b)

Figure 22. Pushdown analysis results of three-storey structures: (a) corner column removed; and (b) middle column removed.

DOI: 10.1002/tal

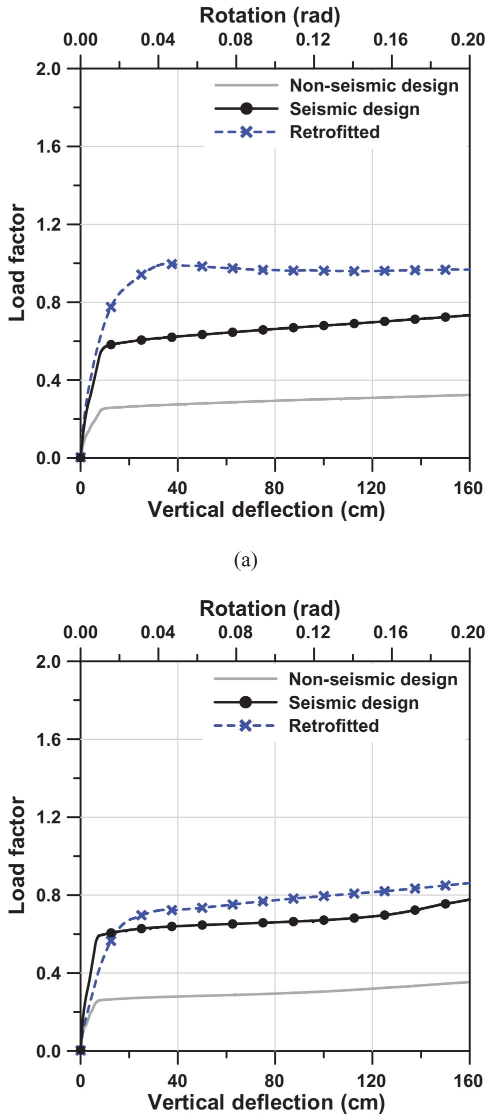

(a)

(b)

Figure 23. Pushdown analysis results of six-storey structures: (a) corner column removed; and (b) middle column removed.

linear static pushdown analysis results of the model structures with one of the first storey column removed. A series of analyses were carried out until the beam rotation reached 0.2 rad based on the observation that the reinforced concrete test specimens of Sasani and Kropelnicki (2008) and Yi *et al.* (2008) failed at similar beam rotation. The progressive collapse-resisting capacity was expressed as a load factor corresponding to a certain vertical deflection level. The load factor of 1.0 implies that the pushdown force reached the loading state specified in the USGSA guideline (2003) including the dynamic amplification factor, $2 \times$ (Dead load $+ 0.25 \times$ Live load). Figure 22 shows the nonlinear static pushdown analysis results of the three-storey structure. When a corner column was removed, the maximum load factor of the OMRF structures not designed for seismic load reached about 0.3. The maximum load factors of the structures designed with seismic load and the structures retrofitted with FDD increased to about 0.5 and 0.9, respectively. When the center column was removed the load

DOI: 10.1002/tal

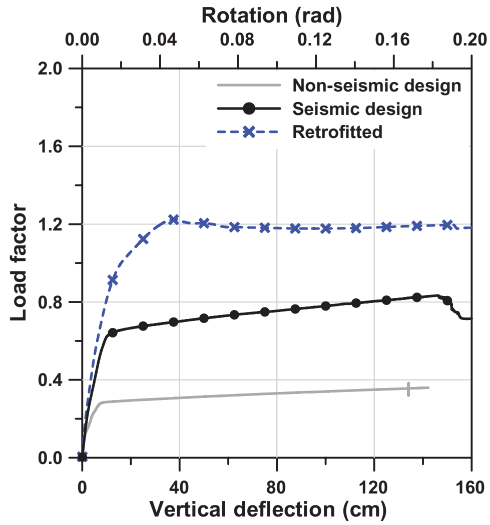

(a)

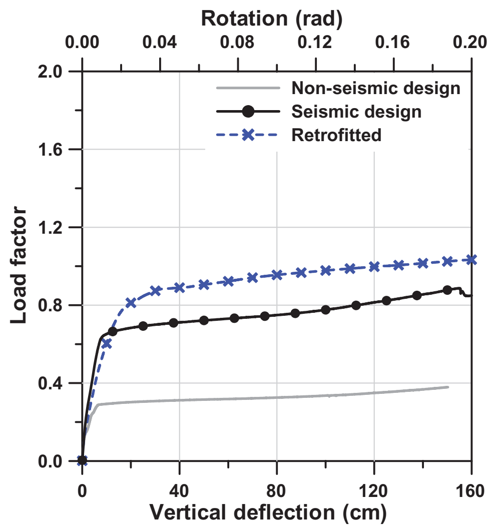

(b)

Figure 24. Pushdown analysis results of 15-storey structures: (a) corner column removed; and (b) Middle column removed.

factors slightly increased due to catenary action of the beams. According to previous research a structure with maximum load factor less than 1.0 may have possibility of progressive collapse due to loss of a column. It was observed that strong possibility of collapse exists in a structure with maximum load factor less than 0.5 (Kim *et al.*, 2009). Therefore, even the structure designed with seismic load turned out to have strong possibility of collapse as a result of the column removal. Figures 23 and 24 present the static pushdown down analysis results of the 6- and 15-storey structures, where it can be observed that as the number of storey increases the maximum load factor of the model structures without dampers slightly increase. However, the maximum load factors of the non-seismic-designed structures are still less than 0.5 and are susceptible to progressive collapse. Even the maximum load factors of the seismic designed structures are still less than 1.0 and are not safe against progressive collapse. On the other hand, the non-seismic-designed structures retrofitted with FDD showed

DOI: 10.1002/tal

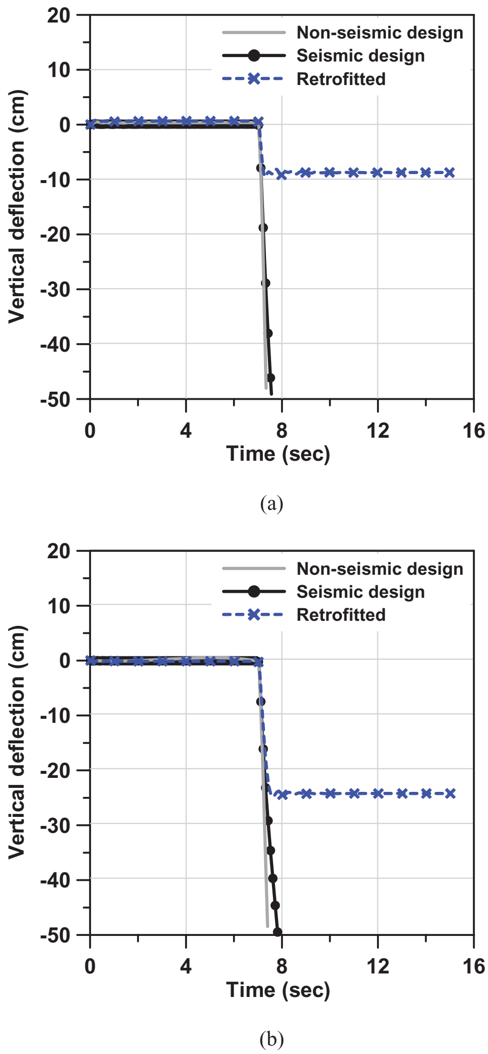

Figure 25. Nonlinear dynamic analysis results of three-storey structures: (a) corner column removed; and (b) middle column removed.

maximum load factors larger than or close to 1.0 and are considered to be safe against progressive collapse.

Figures 25–27 plot the vertical displacement time-histories of the model structures with a corner column and a centre column suddenly removed one at a time. It can be observed that all the model structures not designed for seismic load collapsed after a column was removed, which is consistent with the nonlinear static analysis results. The three-storey seismic designed structure (SMRF) failed when the corner column as well as the centre column was removed. However, both the 6- and 15-storey seismic-designed structures with higher redundancy remained stable after a column was removed. On the other hand, all the model structures retrofitted with FDD turned out to remain stable when a first storey column was removed. The analysis results demonstrate that the FDDs, originally designed to reduce seismic responses, can also be effective in resisting progressive collapse initiated by sudden loss of a column. The effectiveness of the dampers in resisting vertical deflection was higher when a corner column was removed than when a centre column was removed. This is due to the fact that the length of the tendon involved in the vertical deformation in the former case is shorter than that of the latter case.

DOI: 10.1002/tal

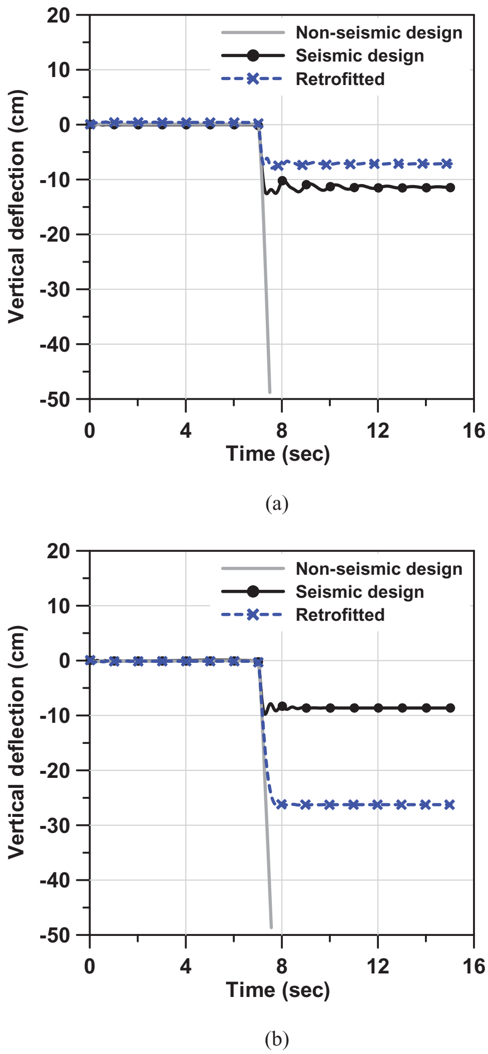

Figure 26. Nonlinear dynamic analysis results of six-storey structures: (a) corner column removed; and (b) middle column removed.

6. CONCLUSIONS

This study presents analytical study of the effectiveness of rotational friction dampers to enhance both seismic- and progressive collapse-resisting capacity of existing structures. To this end 3-, 6- and 15-storey reinforced concrete moment frames were designed as analysis models. The amount of rotational friction dampers required to satisfy given seismic performance limit states was determined using the capacity spectrum method. Nonlinear dynamic time-history analysis results showed that the structures retrofitted with rotational friction dampers generally satisfied the given performance objectives against seismic load. The interstorey drifts of the three-storey structure were generally over-controlled and those of the 15-storey structure were under-controlled due to the seismic retrofit using the capacity spectrum method. The nonlinear static and dynamic analysis results of the model structures with a column suddenly removed showed that the non-seismic-designed model structures and the three-storey seismic-designed structure turned out to collapse after a column was suddenly removed. All the model structures seismically retrofitted by FDDs, however, remained stable no matter which column was removed. This implies that the passive dampers, which have been applied

DOI: 10.1002/tal

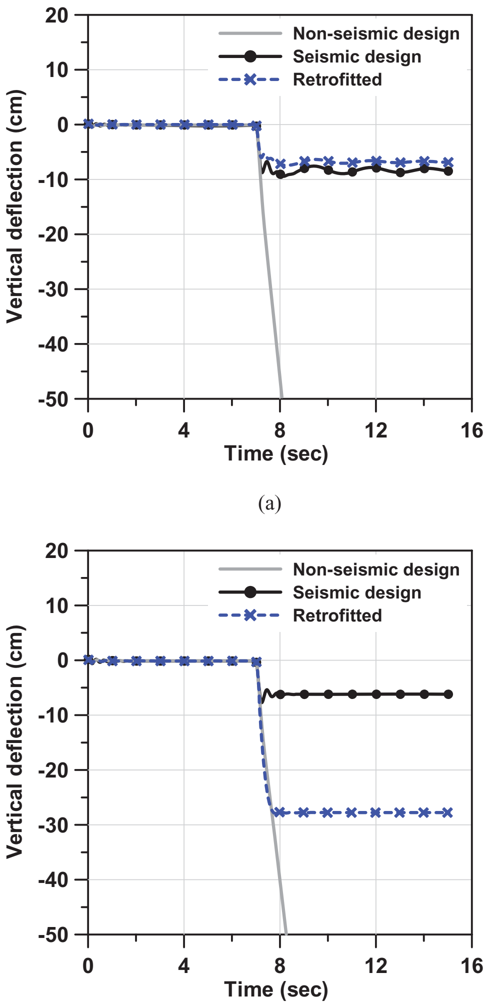

(a)

(b)

Figure 27. Nonlinear dynamic analysis results of 15-storey structures: (a) corner column removed; and (c) middle column removed.

as a means of mitigating wind or earthquake-induced response, may be effective in enhancing progressive collapse-resisting capacity of structures. The effectiveness was more pronounced when a corner column was removed than when a central column was removed.

ACKNOWLEDGEMENT

This research was financially supported by the Super-Tall Building R&D Project of the Ministry of Land, Transport, and Maritime Affairs (09CHUD-A053106-01-000000). The authors are grateful to the authorities for their support.

REFERENCES

ACI 318. 2002. *Building Code Requirements for Structural Concrete (ACI 318-02) and Commentary (318R-02)*. American Concrete Institute: Farmington Hill, MI.

ATC (Applied Technology Council). 1996. *Seismic Evaluation and Retrofit of Concrete Buildings, ATC-40 Report*, ATC: Redwood City, CA.

Bhaskararao AV, Jangid RS. 2006. Seismic analysis of structures connected with friction dampers, *Engineering Structures* **28**(5): 690–703.

Crawford JE. 2002. Retrofit measures to mitigate progressive collapse, *NIST/NIBS, Multihazard Mitigation Council National Workshop on Prevention of Progressive Collapse*, Chicago, IL.

FEMA (Federal Emergency Management Agency). 1997. *NEHRP Guidelines for the Seismic Rehabilitation of Buildings*, Report No. FEMA-273, FEMA: Washington, DC.

Freeman SA, Sasaki K, Paret T. 1998. Multi-mode pushover procedure—A method to identify the effects of higher modes in a pushover analysis. *Proceedings of the 6th National Conference on Earthquake Engineering*, Seattle, WA.

Hayes JR Jr, Woodson SC, Pekelnicky RG, Poland CD, Corley WG, Sozen M. 2005. Can strengthening for earthquake improve blast and progressive collapse resistance? *Journal of Structural Engineering* **131**(8): 1157–1177.

ICC. 2006. *International Building Code*. International Code Council: Falls Church, VA.

Kim J, An D. 2009. Evaluation of progressive collapse potential of steel moment frames considering catenary action. *Structural Design of Tall and Special Buildings* **18**(4): 455–465.

Kim J, Kim T. 2009. Assessment of progressive collapse-resisting capacity of steel moment frames. *Journal of Constructional Steel Research* **65**(1): 169–179.

Kim J, Kim T, Park J. 2009. Investigation of progressive collapse-resisting capability of steel moment frames using push-down analysis. *Journal of Performance of Constructed Facilities* **23**(5): 327–335.

Lee SK, Park JH, Moon BW, Min KW, Lee SH, Kim J. 2008. Design of a bracing-friction damper system for seismic retrofitting. *Smart Structures and Systems* **4**(5): 685–696.

Mander JB, Priestley MJN, Park R. 1988. Theoretical stress-strain model for confined concrete. *Journal of Structural Engineering* **113**(8): 1804–1826.

Mazzoni S, McKenna F, Scott MH, Fenves GL. 2007. *Open System for Earthquake Engineering Simulation*, User Command-Language Manual. Pacific Earthquake Engineering Research Center: Berkeley, CA.

Moreschi LM, Singh MP. 2003. Design of yielding metallic and friction dampers for optimal seismic performance. *Earthquake Engineering & Structural Dynamics* **32**(8): 1291–1311.

Mualla IH, Belev B. 2002. Performance of steel frames with a new friction damper device under earthquake excitation. *Engineering Structures* **24**: 365–371.

NIST (National Institute of Standard and Technology). 2006. *Best Practices for Reducing the Potential for Progressive Collapse in Buildings*. NIST: Gaithersburg, MD.

Pasquin C, Leboeuf AN, Pall AT. 2002. Friction dampers for seismic rehabilitation of Eaton building, Montreal. *Proceeding of the 4th Structural Specialty Conference of the Canadian Society for Civil Engineering*, Montréal, Québec, Canada.

Sasani M, Kropelnicki J. 2008. Progressive collapse analysis of an RC structure. *Structural Design of Tall and Special Buildings* **17**(4): 757–771.

USGSA (U.S. General Services Administration). 2003. *Progressive Collapse Analysis and Design Guidelines for New Federal Office Buildings and Major Modernization Projects.* USGSA: Washington, D.C.

Yi WJ, He QF, Xiao Y, Kunnath SK. 2008. Experimental study on progressive collapse-resistant behavior of reinforced concrete frame structures. *ACI Structural Journal* **105**(4): 433–439.

DOI: 10.1002/tal